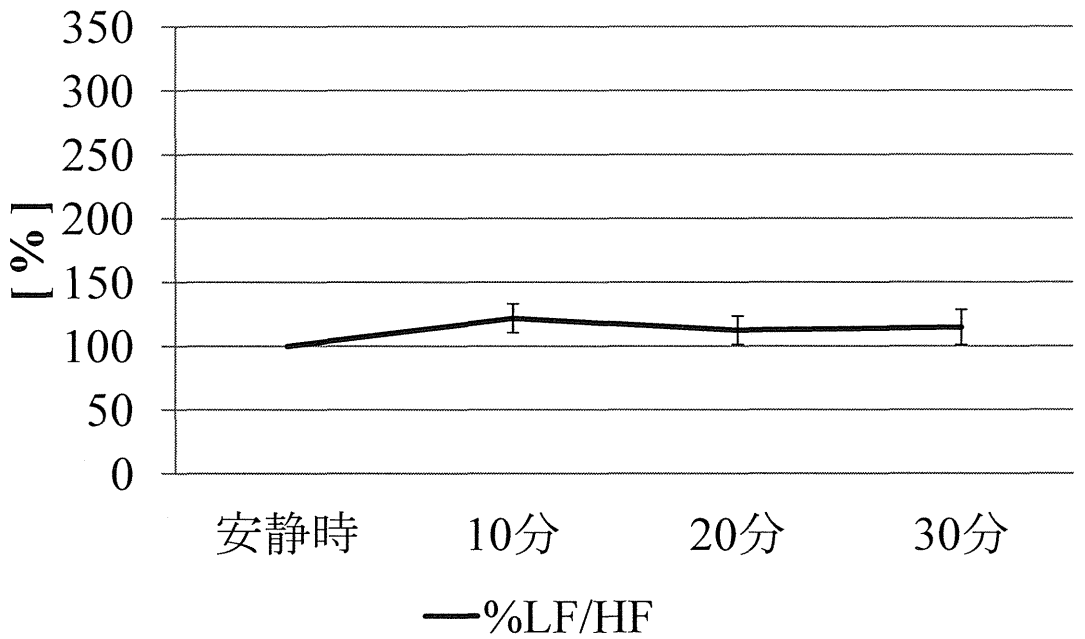

図 16:安静時および足三里穴鍼刺激後 10 分、20 分、30 分における normalized units で表した低周波数領域パワー(LFnorm)の変化を変化率で示す。値は平均±標準誤差で表示。

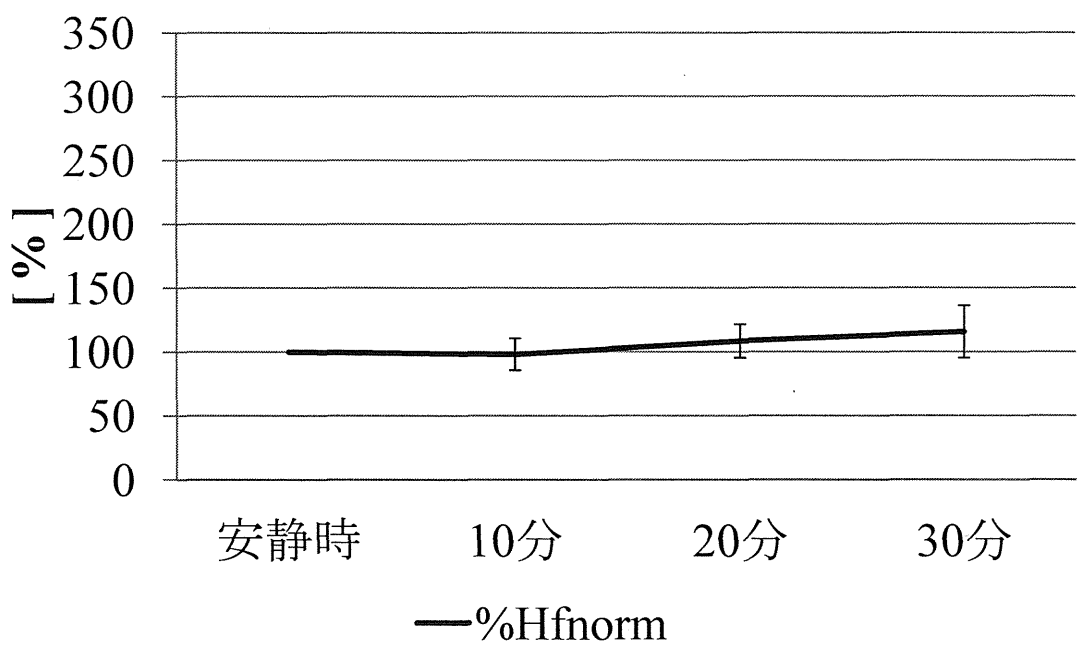

図 17:安静時および足三里穴鍼刺激後 10 分、20 分、30 分における normalized units で表した高周波数領域パワー(HFnorm)の変化を変化率で示す。値は平均±標準誤差で表示。

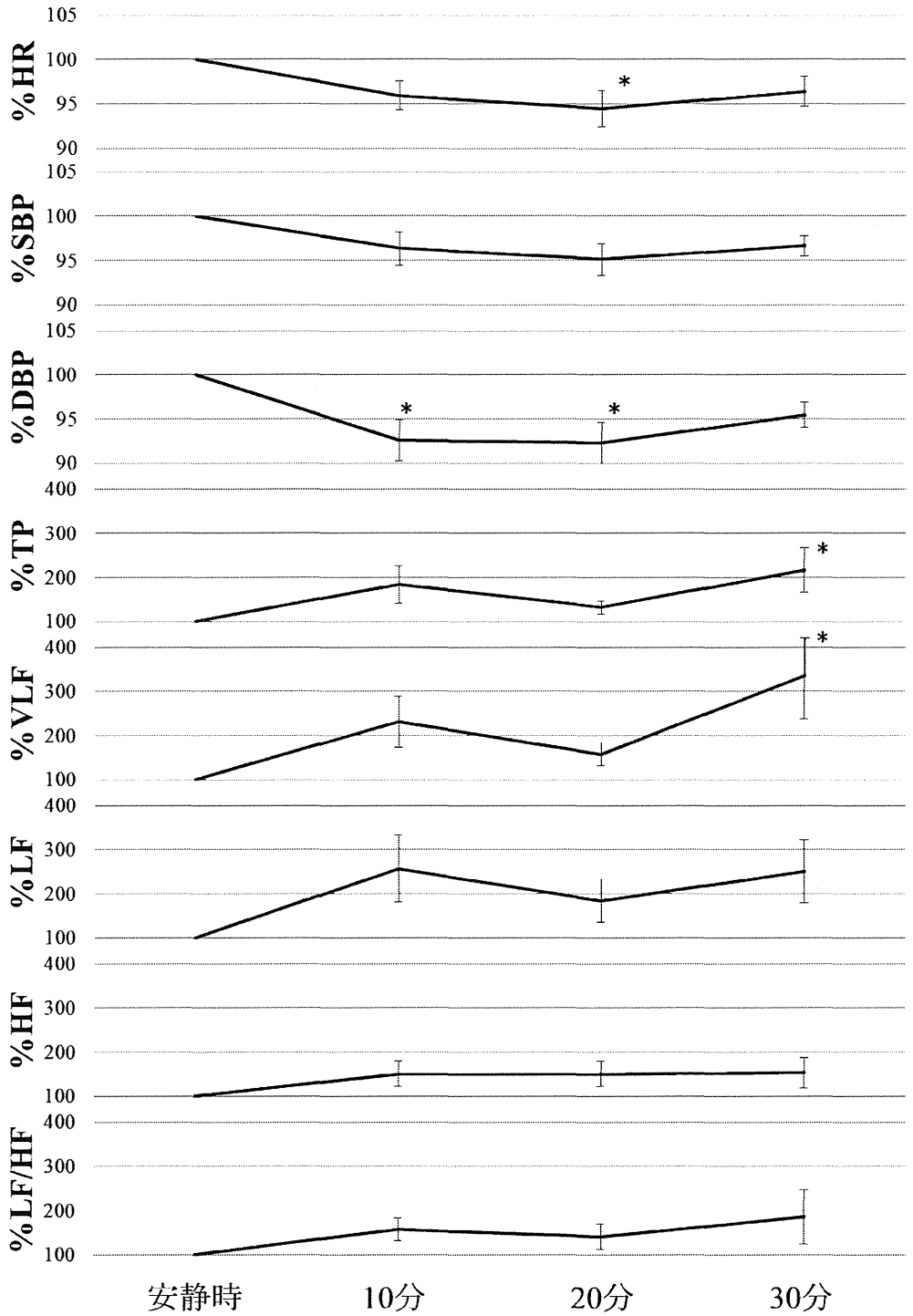

図 18:安静時および足三里穴鍼刺激後 10 分、20 分、30 分における心拍数(HR)、収縮期(SBP)および拡張期(DBP)血圧と各周波数領域のパワー(TP、VLF、LF、HF、LF/HF)を変化率で表す(平均値±標準誤差)。*は安静時と比較して有意な変化を表す(p<0.05)。

Ⅲ. 研究成果の刊行に関する一覧表

研究成果の刊行に関する一覧表

雑誌

発表者氏名	論文タイトル名	発表誌名	巻号	ページ	出版年
阿部　誠，吉澤　誠，テルマ　ケイコ　スガイ，本間　経康，杉田　典大，清水　一夫，後藤　萌，稲垣　正司，杉町　勝，砂川　賢二	植込み型除細動器への実装を考慮した致死性不整脈検出アルゴリズムの改良	電気学会論文誌C,	132(12)	1943-1948	2012
Makoto YOSHIZAWA, Tomoyuki YAMBE, Norihiro SUGITA, Satoshi KONNO, Makoto ABE, Noriyasu HOMMA, Futoshi TAKEI, Katsuhiko YOKOTA, Yoshifumi SAIJO, Shin-ichi NITTA	Application of a Telemedical Tool in an Isolated Island and a Disaster Area of the Great East Japan Earthquake	IEICE TRANSACTIONS on Communications	E95-B(10)	3067-3073	2012
Kenichi Funamoto and Toshiyuki Hayase	Reproduction of pressure field in ultrasonic- measurement-integrated simulation of blood flow	International Journal for Numerical Methods In Biomedical Engineering,	DOI:10.1002/cnm.2522		2012

Ⅳ.研究成果の刊行物・別刷

Hindawi Publishing Corporation
Evidence-Based Complementary and Alternative Medicine
Volume 2012, Article ID 513638, 8 pages
doi:10.1155/2012/513638

Review Article

Evaluation of the Effects of Acupuncture on Blood Flow in Humans with Ultrasound Color Doppler Imaging

Shin Takayama,[1] Masashi Watanabe,[1] Hiroko Kusuyama,[1] Satoru Nagase,[2] Takashi Seki,[1] Toru Nakazawa,[3] and Nobuo Yaegashi[1,2]

[1] *Department of Traditional Asian Medicine, Graduate School of Medicine, Tohoku University, 2-1, Seiryo-machi, Aoba-ku, Sendai 980-8575, Japan*
[2] *Department of Obstetrics and Gynecology, Tohoku University Graduate School of Medicine, Sendai 980-8574, Japan*
[3] *Department of Ophthalmology and Visual Science, Graduate School of Medicine, Tohoku University, Sendai 980-8575, Japan*

Correspondence should be addressed to Shin Takayama, tatahara1492@gmail.com

Received 23 February 2012; Revised 2 April 2012; Accepted 2 April 2012

Academic Editor: Gerhard Litscher

Color Doppler imaging (CDI) can be used to noninvasively create images of human blood vessels and quantitatively evaluate blood flow in real-time. The purpose of this study was to assess the effects of acupuncture on the blood flow of the peripheral, mesenteric, and retrobulbar arteries by CDI. Statistical significance was defined as P values less than 0.05. Blood flow in the radial and brachial arteries was significantly lower during needle stimulation on LR3 than before in healthy volunteers, but was significantly higher after needle stimulation than before. LR3 stimulation also resulted in a significant decrease in the vascular resistance of the short posterior ciliary artery and no significant change of blood flow through the superior mesenteric artery (SMA) during acupuncture. In contrast, ST36 stimulation resulted in a significant increase in blood flow through the SMA and no significant change in the vascular resistance of the retrobulbar arteries. Additionally, acupuncture at previously determined acupoints in patients with open-angle glaucoma led to a significant reduction in the vascular resistance of the central retinal artery and short posterior ciliary artery. Our results suggest that acupuncture can affect blood flow of the peripheral, mesenteric, and retrobulbar arteries, and CDI can be useful to evaluate hemodynamic changes by acupuncture.

1. Introduction

To date, no quantitative evaluation methods have been established for determining the physiological effectiveness of acupuncture. Therefore, researchers conduct experiments using a variety of approaches. In this study, we focused on the physiological reactions to acupuncture and investigated blood flow changes that result from acupuncture [1–5].

Many studies of acupuncture efficacy have been based on the results of animal experiments with anesthesia. These studies indicate that acupuncture works through physiological mechanisms that occur primarily in the autonomic nervous system [6–12]. When acupuncture is performed in human clinical practice, the conditions are very different from those in animal experiments. Additionally, because the invasive examination techniques that are often used to evaluate the results of acupuncture treatments affect the efficacy of those treatments, it is difficult to distinguish physiological reactions caused by acupuncture from those caused by the invasion necessary for examination. To determine the efficacy of acupuncture in humans, it is important that the examination method be noninvasive. We therefore used noninvasive color Doppler imaging (CDI) with ultrasound to evaluate blood flow. CDI is an examination technique that is widely used in the practice and research of Western medicine [13–21]. CDI can quantitatively measure intravascular blood flow in the extremities and in various organs in real-time. It is useful in the investigation of vessels, such as the peripheral, coronary, splenic, adrenal, and superior mesenteric arteries (SMA) [22]. In addition, the reproducibility of real-time and noninvasive hemodynamic measurement with CDI is reported elsewhere [23].

In traditional Chinese medicine, LR3 (Taichong, located on the foot, 1.5–2 units above the web between the

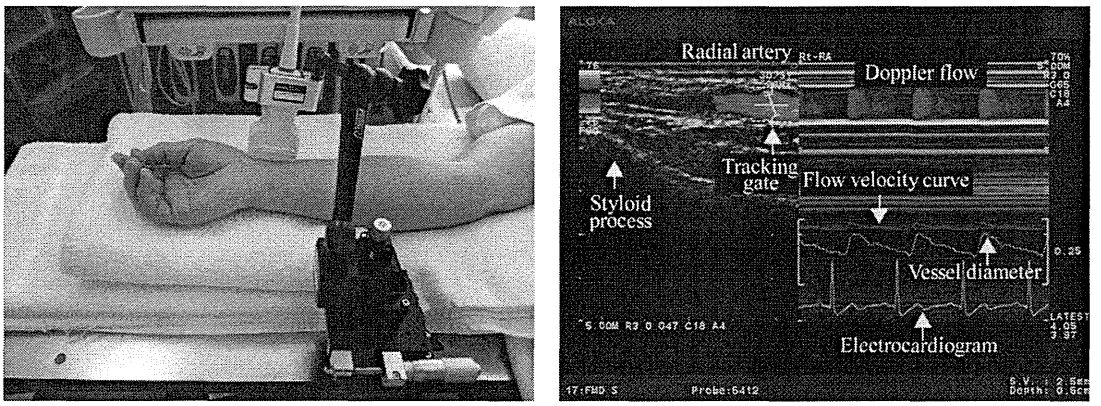

(a) (b)

FIGURE 1: (a) Ultrasound measurement of the radial artery. 13 MHz linear transducer is fixed along radial artery with a special probe holder (MP-PH0001, Aloka Co., Ltd., Tokyo, Japan). (b) Display of CDI. Left: the vessel image and the position of the artery tracking gate. Right: changes in vessel diameter, Doppler flow, and flow velocity as determined by an automated edge-detection device and computer analysis software (e-Tracking system; Aloka Co., Ltd., Tokyo, Japan).

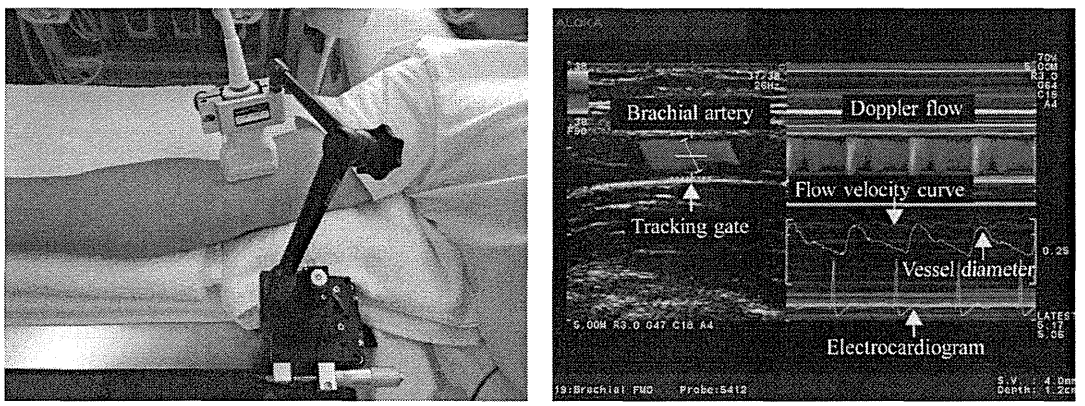

(a) (b)

FIGURE 2: (a) Ultrasound measurement of the brachial artery. 13 MHz linear transducer is fixed along brachial artery with a special probe holder (MP-PH0001, Aloka Co., Ltd., Tokyo, Japan). (b) Display of CDI. Left: image of the vessel image and position of the artery tracking gate. Right: changes in vessel diameter, Doppler flow, and flow velocity, as determined by an automated edge detection device and computer analysis software (e-Tracking system; Aloka Co., Ltd., Tokyo, Japan).

first and second toes [24]) is an acupoint on the liver meridian, which has the functions of "soothing the liver," "regulating the blood," and "opening into the eyes" [24]. We therefore hypothesized that LR3 acupuncture would affect hemodynamics in the peripheral arteries and the retrobulbar arteries. ST36 (Zusanli, located on the lower leg, 3 units below the lateral "eye" of the knee, approximately 1 finger width lateral to the tibia [24]), in contrast, is an acupoint on the stomach meridian, and is associated with the functions of gastrointestinal organs [25]. We therefore hypothesized that ST36 acupuncture would affect hemodynamics in the SMA. Because glaucoma prognosis and retrobulbar circulation are related [26–29], we also investigated the effects of acupuncture on retrobulbar circulation in open-angle glaucoma (OAG) patients. In this study, we introduce the noninvasive CDI with ultrasound to evaluate blood flow changes by acupuncture.

2. Materials and Methods

2.1. Ultrasound Technique for Blood Flow Measurement. We measured circulation in the upper limb, SMA, and retrobulbar vessels using an ultrasound system (Prosound α10; Aloka Co., Ltd, Tokyo, Japan). The system had a 13 MHz linear transducer and a 5 MHz convex transducer. We used the linear transducer to examine peripheral arteries and the retrobulbar vessels. We used the convex transducer to measure SMA circulation.

The radial artery was examined just medial to the radial styloid process (Figure 1). The brachial artery was monitored immediately proximal to the elbow (Figure 2). The SMA supplies blood to the whole small intestine, except for the superior part of the duodenum. It also supplies blood to the cecum, the ascending colon, and most of the transverse colon. SMA measurements were acquired within 2-3 cm of

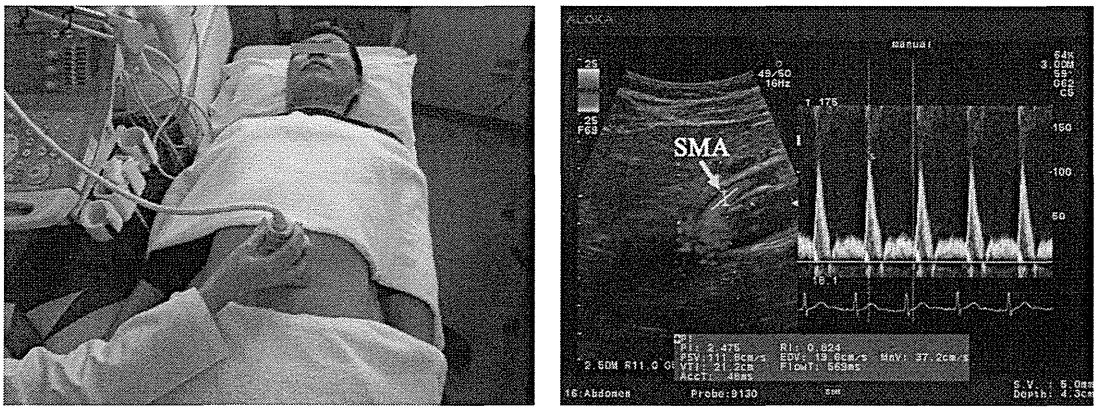

(a) (b)

FIGURE 3: (a) Ultrasound measurement of the SMA. 5 MHz convex transducer is positioned on the abdomen. (b) Display of CDI. Left: image of the vessel and the position of the artery tracking. Right: Doppler flow and flow velocity.

the artery origin (Figure 3) [30, 31]. Avoiding any pressure on the eye, CDI was performed for the retrobulbar vessels, including the ophthalmic artery (OA), central retinal artery (CRA), and nasal or temporal short posterior ciliary artery (Figures 4 and 5). The OA was examined approximately 20 mm behind the globe (Figure 5(b)), the CRA was examined within 5 mm of the retrolaminar portion of the optic nerve (Figure 5(c)), and the nasal or temporal SPCA that obtained clear image was examined approximately 5–10 mm behind the globe (Figure 5(d)). Blood flow was monitored continuously [32, 33] and we employed a Doppler angle of 60° or less for each measurement [34, 35]. Each Doppler waveform was automatically drawn and calculated using the software included with the ultrasound system. The following calculations were used to determine the hemodynamic parameters at each site [30, 31].

(i) Vessel diameter (VD).

(ii) Cross-sectional area (CSA) = $(VD/2)^2 \times \pi$.

(iii) Peak systolic velocity (PSV).

(iv) End-diastolic velocity (EDV).

(v) Resistive index (RI) = (PSV − EDV)/PSV.

(vi) Mean flow velocity (MV).

(vii) Blood flow volume = CSA × MV.

2.2. Statistical Analysis. Statistical analysis was performed with SPSS software (version 16.0, SPSS Japan Inc., Tokyo, Japan). Repeated measure analysis of variance, followed by Dunnett's post hoc test, was used for statistical comparison between the measure points. Comparison between rest and after acupuncture was done by paired t-test. Results are presented as the mean ± SD and $P < 0.05$ was taken to indicate significance for all statistical analysis.

2.3. Experiment 1: Effects of LR3 Acupuncture on Upper Limb Circulation [1]. This study was employed to investigate the upper limb circulation after acupuncture at LR3 acupoints on foot. The participants were recruited by the poster recruitment in Tohoku University. Eighteen healthy volunteers (mean age: 32 ± 5 years; 14 males and 4 females) were enrolled in this study. A disposable fine stainless-steel needle (diameter: 0.16 mm; length: 40 mm; Seirin Co., Ltd., Shizuoka, Japan) was inserted on LR3 bilaterally and maintained at a depth of 10 mm during the test. After the needle was inserted, stimulation (rotating the needles manually within an angle of 90 degrees) was performed for 18 seconds. The needles were removed 200 seconds after acupuncture. Radial and brachial CDI were performed before acupuncture; during acupuncture treatment; 30, 60, and 180 seconds after acupuncture.

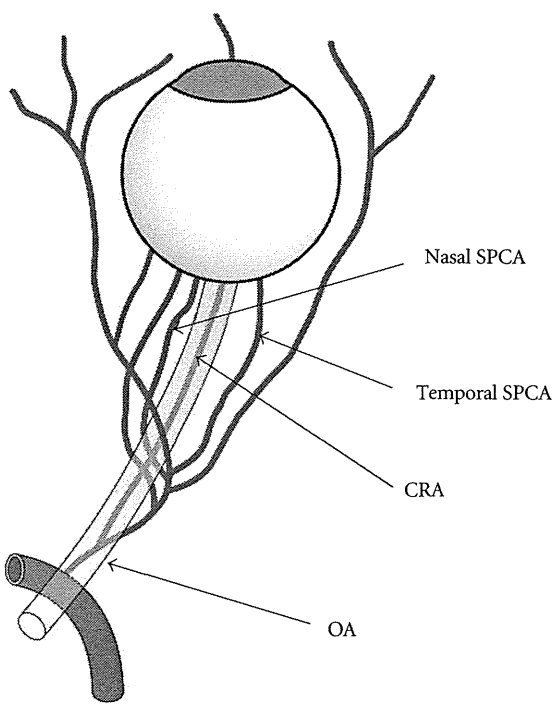

FIGURE 4: Schema of the retrobulbar arteries (OA: ophthalmic artery, CRA: central retinal artery, and SPCA: short posterior ciliary artery).

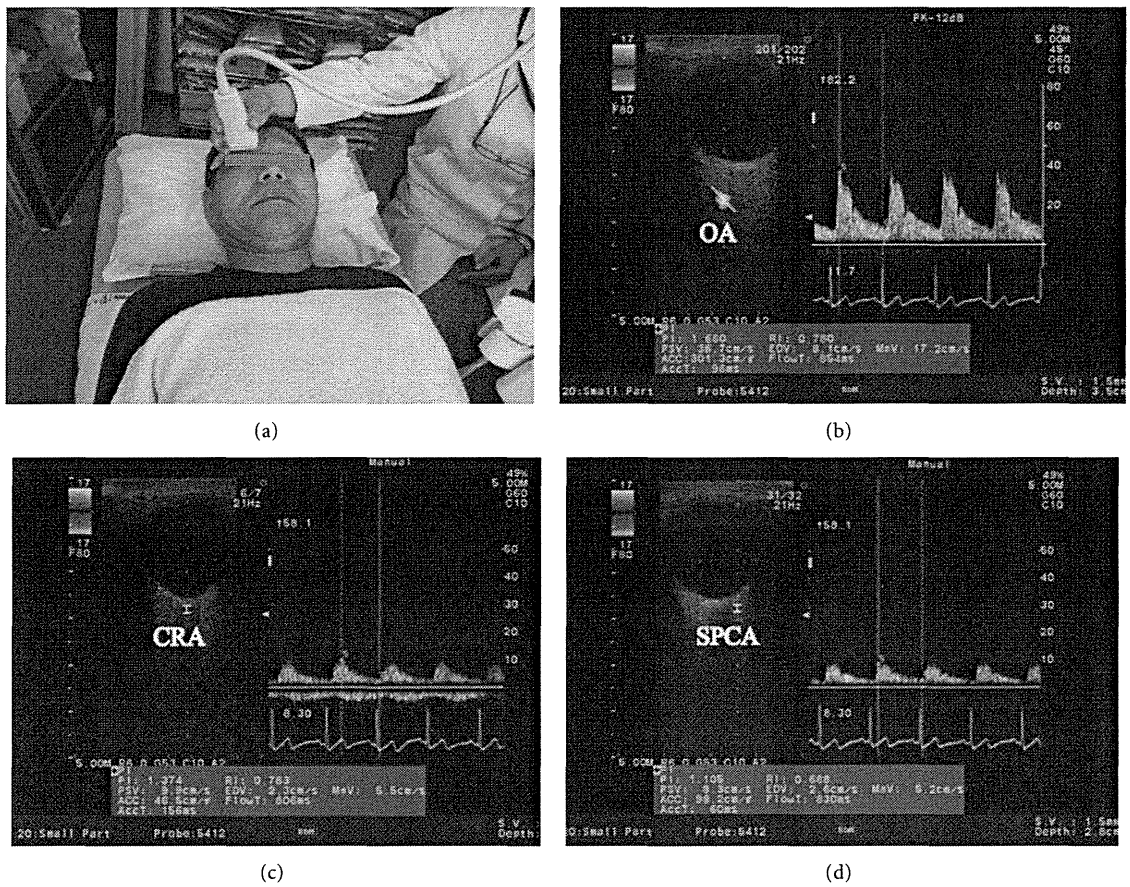

FIGURE 5: (a) Ultrasound measurement of retrobulbar arteries. 13 MHz linier transducer is attached on the eyelid. Horizontal scans by CDI through the ocular globe showing the (b) ophthalmic artery (OA), (c) central retinal artery (CRA), and (d) temporal short posterior ciliary artery (SPCA). Left: image of the vessel and the position of the artery tracking. Right: Doppler flow and flow velocity (b, c, and d).

2.4. Experiment 2: Effects of LR3 Acupuncture on Blood Circulation to the Eye and through the SMA. This study was employed to clarify the hemodynamic changes by acupuncture in two different organs (intestine and eye) with simultaneous evaluation by ultrasound. The participants were recruited by the poster recruitment in Tohoku University. Thirteen healthy volunteers (mean age: 36 ± 9 years; 10 males and 3 females) were enrolled in this study. Acupuncture was performed bilaterally on LR3 with manual needle rotation and the disposable stainless steel needles (0.16 mm × 40 mm; Seirin Co. Ltd., Shizuoka, Japan) were kept at the same site for 15 minutes. Retrobulbar vessels and SMA circulation were measured simultaneously at rest and 15 minutes after the start of acupuncture using ultrasound.

2.5. Experiment 3: Effects of ST36 Acupuncture Blood Circulation to the Eye and through the SMA. This study was also employed to clarify the hemodynamic changes by acupuncture in two different organs (intestine and eye) with simultaneous evaluation by ultrasound. The participants were recruited by the poster recruitment in Tohoku University. Thirteen subjects (mean age: 36 ± 8 years; 10 males and 3 females) were enrolled in this study. Acupuncture was performed bilaterally on ST36 with manual rotation of the disposable stainless steel needles (0.16 mm × 40 mm; Seirin Co. Ltd., Shizuoka, Japan) were kept in the same site for 15 minutes. Retrobulbar vessels and SMA circulation were measured simultaneously at rest and 15 minutes after the start of acupuncture using ultrasound.

2.6. Experiment 4: Effects of Acupuncture on Retrobulbar Circulation in OAG Patients [2]. The relation between glaucoma and retrobulbar circulation in the prognosis of the disease has been indicated [26–29], therefore we investigated the effects of acupuncture on OAG patients by CDI. The patients were recruited in the outpatient clinic of ophthalmology in Tohoku University Hospital. Eleven OAG patients (mean age: 63 ± 11 years; 1 male and 10 females; 20 eyes with OAG) were enrolled. All patients included in the study had been treated with topical antiglaucoma medications for at least 3 months prior to the study. As a control, the subjects received the measurements of retrobulbar vessel hemodynamics that were performed at rest and one hour after the first measurement. One month later, they received the same measurements before and after acupuncture treatment. Acupuncture was performed once bilaterally at acupoints BL2, EX-HN5, ST2, ST36, SP6, KI3, LR3, GB20, BL18, and BL23 for 15 minutes using disposable stainless steel needles

Table 1: Hemodynamic parameters and blood flow volume of the radial and brachial arteries by acupuncture on LR3. The values represent the mean and SD. $^{*}P < 0.05$, $^{**}P < 0.01$ versus before acupuncture. Modified from [1].

Parameters	Acupuncture on LR3				
	Before	During	30 s after	60 s after	180 s after
Systolic blood pressure (mmHg)	116.8 ± 10.1				114.5 ± 12.3
Diastolic blood pressure (mmHg)	67.3 ± 8.4				65.8 ± 7.3
Heart rate (beats/min)	67.3 ± 10.1	64.2 ± 8.8	65.8 ± 9.3	66.2 ± 9.3	66.9 ± 9.6
Blood flow volume of the radial artery (mL/min)	56.3 ± 33.5	25.4 ± 26.3	57.9 ± 47.5	67.7 ± 44.7	67.0 ± 36.5
Blood flow volume of the brachial artery (mL/min)	87.5 ± 56.4	65.7 ± 41.6	86.8 ± 53.7	90.1 ± 51.5	106.5 ± 59.8

Table 2: Hemodynamic parameters, blood flow volume of the SMA, and resistive index of retrobulbar arteries by acupuncture on LR3. The values represent the mean and SD. $^{*}P < 0.05$, $^{**}P < 0.01$ versus before acupuncture.

Parameters	Acupuncture on LR3	
	Before	After
Systolic blood pressure (mmHg)	119.6 ± 12.8	116.7 ± 11.1
Diastolic blood pressure (mmHg)	77.7 ± 9.4	76.5 ± 9.3
Heart rate (beats/min)	66.8 ± 7.1	63.3 ± 4.6**
Blood flow volume of the SMA (mL/min)	734.8 ± 312.9	704.4 ± 328.1
RI in OA	0.719 ± 0.097	0.707 ± 0.089
RI in CRA	0.661 ± 0.088	0.644 ± 0.052
RI in SPCA	0.624 ± 0.057	0.580 ± 0.037*

(0.16 mm or 0.20 mm × 40 mm; Seirin Co. Ltd., Shizuoka, Japan). Retrobulbar circulation was measured using CDI at rest prior to treatment and 1 hour later, or after acupuncture.

3. Results and Discussion

3.1. Experiment 1: Effects of LR3 Acupuncture on Upper Limb Circulation [1]. Hemodynamic parameters including blood pressure, heart rate, and blood flow volume in the radial and brachial arteries are summarized in Table 1. Figure 6 illustrates the profile of the percent changes in blood flow volume in the radial and brachial arteries. The blood flow volume in the radial artery decreased significantly during acupuncture ($P < 0.01$), but showed a significant increase at 180 seconds after acupuncture ($P < 0.05$) (Figure 6). In the brachial artery, the blood flow volume also showed a significant increase at 180 seconds after acupuncture ($P < 0.05$) (Figure 6). The physiological mechanisms of decrease and increase blood flow volume in upper limb are presumably related to a peripheral vascular resistance due to an instantaneous increase and decrease in sympathetic tone [1]. The present result suggests that LR3 located on the foot and apart from the upper limb can affect the circulation in the upper limb.

3.2. Experiment 2: Effects of LR3 Acupuncture on Blood Circulation to the Eye and through the SMA. The RI of the SPCA was significantly lower after acupuncture than before ($P < 0.05$; Table 2). However, blood flow volume in the SMA was not significantly changed after acupuncture than before (Table 2). The SPCA is the ocular branches of the OA and it supplies blood to the choroid (Figure 4) [32]. The decrease of the distal vascular resistance in the SPCA that

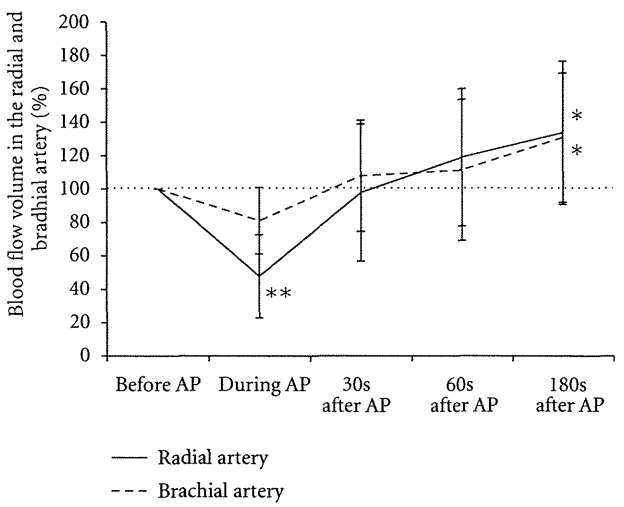

Figure 6: Percent changes in blood flow volume in the radial and brachial arteries before, during, and after acupuncture treatment. Values are presented as a percentage of the pretreatment blood flow. Values represent the mean and SD. AP: acupuncture. $^{*}P < 0.05$, $^{**}P < 0.01$ versus before acupuncture. Modified from [1].

we observed indicates that acupuncture on LR3 results in an increase of the blood flow to the choroid. It has been reported that the blood flow in the eye is controlled by sympathetic and parasympathetic nerves, and it is related with the release of nitric oxide or calcitonin gene-related peptide [33, 34]; it has also been reported that the regulation of regional blood flow by somatic afferent stimulation is based on somatoautonomic reflex mechanisms in the choroidal blood flow of the eyeball [34]. The hemodynamic changes in the SPCA by acupuncture may be related with these

Table 3: Hemodynamic parameters, blood flow volume of the SMA, and resistive index of retrobulbar arteries by acupuncture on ST36. The values represent the mean and SD. $^{*}P < 0.05$, $^{**}P < 0.01$ versus before acupuncture.

Parameters	Acupuncture on ST36	
	Before	After
Systolic blood pressure (mmHg)	121.7 ± 11.8	120.7 ± 10.9
Diastolic blood pressure (mmHg)	77.8 ± 9.4	77.6 ± 7.6
Heart rate (beats/min)	61.9 ± 6.6	61.5 ± 7.4
Blood flow volume of the SMA (mL/min)	549.8 ± 192.2	620.2 ± 188.1*
RI in OA	0.736 ± 0.07	0.728 ± 0.070
RI in CRA	0.617 ± 0.065	0.631 ± 0.043
RI in SPCA	0.600 ± 0.030	0.580 ± 0.06

Table 4: Hemodynamic parameters and resistive index of retrobulbar arteries in control and acupuncture therapy. The values represent the mean and SD. $^{*}P < 0.05$, $^{**}P < 0.01$ versus rest or before acupuncture. $^{\dagger}P < 0.05$, $^{\dagger\dagger}P < 0.01$ versus control. Modified from [2].

Parameters	Control		Acupuncture	
	Rest	After 1 hour	Before	After
Systolic blood pressure (mmHg)	116.4 ± 10.0	119.8 ± 7.6	124.5 ± 12.9	122.6 ± 9.7
Diastolic blood pressure (mmHg)	69.8 ± 6.5	68.6 ± 3.9	74.5 ± 5.4	72.0 ± 2.9
Heart rate (beats/min)	61.5 ± 7.3	60.1 ± 8.1	61.7 ± 8.5	60.3 ± 10.4
RI in OA	0.74 ± 0.04	0.75 ± 0.05	0.74 ± 0.04	0.74 ± 0.04
RI in CRA	0.75 ± 0.09	0.72 ± 0.03	0.72 ± 0.05	0.68 ± 0.04*
RI in SPCA	0.68 ± 0.05	0.68 ± 0.04	0.67 ± 0.04	0.64 ± 0.06*††

mechanisms. The present result suggests that LR3 located on the foot and apart from the eye can affect the circulation in the retrobulbar arteries.

3.3. Experiment 3: Effects of ST36 Acupuncture on Blood Circulation to the Eye and through the SMA. RI in the retrobulbar vessels was not changed by ST36 acupuncture treatment. However, the blood flow volume in the SMA was significantly greater after acupuncture than before ($P < 0.05$; Table 3). Acupuncture on the limbs was also demonstrated to elicit systemic visceral responses via the supraspinal reflexes in animal models [9, 36, 37]. According to several reports, blood flow volume in the SMA increased significantly after stimulation of the lower limbs [9, 36–38]. We speculate that this increase is caused by excitation of the parasympathetic system and inhibition of the sympathetic system via supraspinal reflexes. The present result suggests that ST36 located on the lower limb and apart from the abdomen can affect the circulation in the SMA.

3.4. Experiment 4: Effects of Acupuncture on Retrobulbar Circulation in OAG Patients. RI in the CRA and SPCA were significantly lower after acupuncture than it was before acupuncture treatment (CRA; $P < 0.05$, SPCA; $P < 0.05$; Table 4). RI in the SPCA was also significantly lower after acupuncture than when no treatment was given (SPCA; $P < 0.01$; Table 4). The CRA supplies blood to the retina and SPCA, to the choroid (Figure 4). The decrease of the distal vascular resistance in the CRA and SPCA that we observed indicates that acupuncture results in an increase of the blood flow to the retina and choroid. The possible physiological mechanisms of increase blood flow in eye has already described in the discussion of Experiment 2. The present result suggests that acupuncture can improve the retrobulbar circulation in the patients of OAG with standard medication.

4. Ultrasound and CDI

4.1. Advantage. We focused on the evaluation of CDI by ultrasound. Noninvasive and real-time measure of CDI was applied to assess circulation in organs after acupuncture. The continuous method of CDI was used to assess the brief effects of circulation in the arm (Experiment 1). The simultaneous evaluation by CDI was applied to assess the circulation in two different organs (Experiments 2 and 3). Resistive index measured by CDI is measured in the small vessels as retrobulbar arteries (Experiment 4). Acupuncture affects the autonomic nervous system via the somatic nerves. Invasive evaluation also affects these systems and reflex. Therefore, invasive evaluation might not correctly evaluate the physiological effects of acupuncture therapy. We suggest that real-time and noninvasive hemodynamic measurement as CDI is suitable to measure the physiological effects in humans.

4.2. Limitation. While CDI provides detailed images of blood vessels in real-time, there are limits to the hemodynamic measurements that can be made using this technique. In addition, while CDI is useful for the measurement of blood flow in various vessels in real time, it does not have sufficient resolution to determine the diameter of very small retrobulbar vessels such as OA, CRA, and SPCA. Therefore,

CDI cannot be used to measure blood flow volume in these vessels. However, it can provide an index of vascular resistance such as RI. A decrease in the distal vascular resistance in the small vessels indicates an increase in the blood flow in the distal part of the vessels. Additionally, care must be taken to avoid compression of the eyeball during ultrasound examination. Such compression is likely to cause intraocular pressure elevation and trigger the vagal reflex. Measurement of blood flow in the retrobulbar arteries requires attention to probe maintenance and careful avoidance of pressure on the eyeball [23]. Expert technique is required to obtain reproducible results using CDI. In addition to the limits of CDI resolution, ultrasound waves that strike blood vessels at angles greater than 60° relative to the direction of blood flow result in a large margin of error for CDI measurements. Therefore, it is important to measure blood flow at a Doppler angle of less than 60 degrees [34, 35].

4.3. Further Study. The other methods to assess the physiological changes by acupuncture noninvasively are impedance cardiography and spectral analysis of heart rate variability. Impedance cardiography is a noninvasive monitoring method that allows measurement of the cardiac index based on the changes in thoracic resistance that results from variations in intrathoracic blood flow volume [39, 40]. Spectral analysis of heart rate variability is useful to evaluate the autonomic nervous balance noninvasively [41, 42]. Combined with these measurements, we can clarify the mechanism of increased blood flow volume in several organs in humans. In the future, we would like to explore the efficacy of acupuncture as treatment for various diseases by using diagnostic tools, such as CDI.

5. Conclusion

CDI can noninvasively depict blood vessels in the human body, and can quantitatively evaluate blood flow in real time. Our studies showed the changes of blood flow in the peripheral, mesenteric, and retrobulbar arteries by acupuncture estimated by CDI. This technique is suitable as an evaluation method to consider physiological changes due to acupuncture as blood flow changes.

Conflict of Interests

The authors have no conflict of interests.

Acknowledgments

Experiment 1 was supported by Special Coordination Funds for Promoting Science and Technology from the Japanese Ministry of Education, Culture, Sports, Science and Technology. Experiment 4 was supported by Health and Labour Sciences Research Grants for Clinical Research from the Japanese Ministry of Health, Labour and Welfare.

References

[1] S. Takayama, T. Seki, M. Watanabe et al., "Brief effect of acupuncture on the peripheral arterial system of the upper limb and systemic hemodynamics in humans," *Journal of Alternative and Complementary Medicine*, vol. 16, no. 7, pp. 707–713, 2010.

[2] S. Takayama, T. Seki, T. Nakazawa et al., "Short-term effects of acupuncture on open-angle glaucoma in retrobulbar circulation: additional therapy to standard medication," *Evidence-Based Complementary and Alternative Medicine*, vol. 2011, Article ID 157090, 6 pages, 2011.

[3] S. Takayama, T. Seki, M. Watanabe et al., "Changes of blood flow volume in the superior mesenteric artery and brachial artery with abdominal thermal stimulation," *Evidence-Based Complementary and Alternative Medicine*, vol. 2011, Article ID 214089, 10 pages, 2011.

[4] S. Takayama, T. Seki, N. Sugita et al., "Radial artery hemodynamic changes related to acupuncture," *Explore*, vol. 6, no. 2, pp. 100–105, 2010.

[5] S. Takayama, T. Seki, M. Watanabe et al., "The effect of warming of the abdomen and of herbal medicine on superior mesenteric artery blood flow—a pilot study," *Forschende Komplementarmedizin*, vol. 17, no. 4, pp. 195–201, 2010.

[6] D. Irnich and A. Beyer, "Neurobiological mechanisms of acupuncture analgesia," *Schmerz*, vol. 16, no. 2, pp. 93–102, 2002.

[7] J. G. Lin and W. L. Chen, "Acupuncture analgesia: a review of its mechanisms of actions," *American Journal of Chinese Medicine*, vol. 36, no. 4, pp. 635–645, 2008.

[8] Z. Q. Zhao, "Neural mechanism underlying acupuncture analgesia," *Progress in Neurobiology*, vol. 85, no. 4, pp. 355–375, 2008.

[9] S. Uchida and H. Hotta, "Acupuncture affects regional blood flow in various organs," *Evidence-Based Complementary and Alternative Medicine*, vol. 5, no. 2, pp. 145–151, 2008.

[10] H. Tsuru and K. Kawakita, "Acupuncture on the blood flow of various organs measured simultaneously by colored microspheres in rats," *Evidence-Based Complementary and Alternative Medicine*, vol. 6, no. 1, pp. 77–83, 2009.

[11] E. Haker, H. Egekvist, and P. Bjerring, "Effect of sensory stimulation (acupuncture) on sympathetic and parasympathetic activities in healthy subjects," *Journal of the Autonomic Nervous System*, vol. 79, no. 1, pp. 52–59, 2000.

[12] Y. Syuu, H. Matsubara, T. Kiyooka et al., "Cardiovascular beneficial effects of electroacupuncture at Neiguan (PC-6) acupoint in anesthetized open-chest dog," *Japanese Journal of Physiology*, vol. 51, no. 2, pp. 231–238, 2001.

[13] J. Soga, K. Nishioka, S. Nakamura et al., "Measurement of flow-mediated vasodilation of the brachial artery—a comparison of measurements in the seated and supine positions," *Circulation Journal*, vol. 71, no. 5, pp. 736–740, 2007.

[14] J. Deanfield, A. Donald, C. Ferri et al., "Endothelial function and dysfunction. Part I: methodological issues for assessment in the different vascular beds: a statement by the working group on endothelin and endothelial factors of the European society of hypertension," *Journal of Hypertension*, vol. 23, no. 1, pp. 7–17, 2005.

[15] J. Kjeldsen and O. B. Schaffalitzky de Muckadell, "Assessment of disease severity and activity in inflammatory bowel disease," *Scandinavian Journal of Gastroenterology*, vol. 28, no. 1, pp. 1–9, 1993.

[16] M. J. Perko, "Duplex ultrasound for assessment of superior mesenteric artery blood flow," *European Journal of Vascular and Endovascular Surgery*, vol. 21, no. 2, pp. 106–117, 2001.

[17] G. L. Moneta, D. C. Taylor, W. S. Helton, M. W. Mulholland, and D. E. Strandness, "Duplex ultrasound measurement of postprandial intestinal blood flow: effect of meal composition," *Gastroenterology*, vol. 95, no. 5, pp. 1294–1301, 1988.

[18] A. Erden, T. Cumhur, and T. Ölçer, "Superior mesenteric artery Doppler waveform changes in response to inflammation of the ileocecal region," *Abdominal Imaging*, vol. 22, no. 5, pp. 483–488, 1997.

[19] M. F. Byrne, M. A. Farrell, S. Abass et al., "Assessment of Crohn's disease activity by Doppler sonography of the superior mesenteric artery, clinical evaluation and the Crohn's disease activity index: a prospective study," *Clinical Radiology*, vol. 56, no. 12, pp. 973–978, 2001.

[20] A. Sigirci, T. Baysal, R. Kutlu et al., "Doppler sonography of the inferior and superior mesenteric arteries in ulcerative colitis," *Journal of Clinical Ultrasound*, vol. 29, no. 3, pp. 130–139, 2001.

[21] C. R. Deane and H. S. Markus, "Colour velocity flow measurement: in vitro validation and application to human carotid arteries," *Ultrasound in Medicine and Biology*, vol. 23, no. 3, pp. 447–452, 1997.

[22] U. Gembruch, "Assessment of the fetal circulatory state in uteroplacental insufficiency by Doppler ultrasound: which vessels are the most practicable?" *Ultrasound in Obstetrics and Gynecology*, vol. 8, no. 2, pp. 77–81, 1996.

[23] E. T. Matthiessen, O. Zeitz, G. Richard, and M. Klemm, "Reproducibility of blood flow velocity measurements using colour decoded Doppler imaging," *Eye*, vol. 18, no. 4, pp. 400–405, 2004.

[24] D. Bensky and J. O'Connor, *Acupuncture a Comprehensive Text*, Eastland Press, Seattle, Wash, USA, 1981.

[25] M. Giovanni, *The Moundations of Chinese Medicine*, Churchill Livingstone, Philadelphia, Pa, USA, 1989.

[26] Y. Yamazaki and S. M. Drance, "The relationship between progression of visual field defects and retrobulbar circulation in patients with glaucoma," *American Journal of Ophthalmology*, vol. 124, no. 3, pp. 287–295, 1997.

[27] I. Stalmans, A. Harris, S. Fieuws et al., "Color Doppler imaging and ocular pulse amplitude in glaucomatous and healthy eyes," *European Journal of Ophthalmology*, vol. 19, no. 4, pp. 580–587, 2009.

[28] M. Satilmis, S. Orgül, B. Doubler, and J. Flammer, "Rate of progression of glaucoma correlates with retrobulbar circulation and intraocular pressure," *American Journal of Ophthalmology*, vol. 135, no. 5, pp. 664–669, 2003.

[29] J. Schumann, S. Orgül, K. Gugleta, B. Dubler, and J. Flammer, "Interocular difference in progression of glaucoma correlates with interocular differences in retrobulbar circulation," *American Journal of Ophthalmology*, vol. 129, no. 6, pp. 728–733, 2000.

[30] R. W. Gill, "Measurement of blood flow by ultrasound: accuracy and sources of error," *Ultrasound in Medicine and Biology*, vol. 11, no. 4, pp. 625–641, 1985.

[31] F. Van Bel, P. H. T. Van Zwieten, G. L. Guit, and J. Schipper, "Superior mesenteric artery blood flow velocity and estimated volume flow: duplex Doppler US study of preterm and term neonates," *Radiology*, vol. 174, no. 1, pp. 165–169, 1990.

[32] K. Mayumi, "Aiming at a wide range of applications from preventive medicine to treatment," *Innervision*, vol. 21, no. 4, pp. 20–21, 2006.

[33] O. Takashi, "Measurement of minimal changes in blood vessels and its application," *Journal of Clinical Echocardiography*, vol. 7, no. 11, pp. 936–941, 2006.

[34] P. N. Burns and C. C. Jaffe, "Quamtitative flow measurements with Doppler ultrasound: techniques, accuracy, and limitations," *Radiologic Clinics of North America*, vol. 23, no. 4, pp. 641–657, 1985.

[35] K. J. W. Taylor and S. Holland, "Doppler US. Part I. Basic principles, instrumentation, and pitfalls," *Radiology*, vol. 174, no. 2, pp. 297–307, 1990.

[36] A. Sato, Y. Sato, A. Suzuki, and S. Uchida, "Reflex modulation of catecholamine secretion and adrenal sympathetic nerve activity by acupuncture-like stimulation in anesthetized rat," *Japanese Journal of Physiology*, vol. 46, no. 5, pp. 411–421, 1996.

[37] E. Noguchi, "Mechanism of reflex regulation of the gastroduodenal function by acupuncture," *Evidence-Based Complementary and Alternative Medicine*, vol. 5, no. 3, pp. 251–256, 2008.

[38] M. Watanabe, S. Takayama, T. Seki et al., "Haemodynamic changes in the superior mesenteric artery induced by acupuncture stimulation on the lower limbs," *Evidence-Based Complementary and Alternative Medicine*. In press.

[39] A. C. Perrino, A. Lippman, C. Ariyan, T. Z. O'Connor, and M. Luther, "Intraoperative cardiac output monitoring: comparison of impedance cardiography and thermodilution," *Journal of Cardiothoracic and Vascular Anesthesia*, vol. 8, no. 1, pp. 24–29, 1994.

[40] N. M. Albert, M. D. Hail, J. Li, and J. B. Young, "Equivalence of the bioimpedance and thermodilution methods in measuring cardiac output in hospitalized patients with advanced, decompensated chronic heart failure," *American Journal of Critical Care*, vol. 13, no. 6, pp. 469–479, 2004.

[41] S. Lee, Y. Chae, S. N. Kim et al., "Short term effects by acupuncture to SP3 on the autonomic blood flow control," *Neurological Research*, vol. 32, no. 1, pp. S37–S42, 2010.

[42] J. H. Lee, K. H. Kim, J. W. Hong, W. C. Lee, and S. Koo, "Comparison of electroacupuncture frequency-related effects on heart rate variability in healthy volunteers: a randomized clinical trial," *Journal of Acupuncture and Meridian Studies*, vol. 4, no. 2, pp. 107–115, 2011.

INTERNATIONAL JOURNAL FOR NUMERICAL METHODS IN BIOMEDICAL ENGINEERING
Int. J. Numer. Meth. Biomed. Engng. (2012)
Published online in Wiley Online Library (wileyonlinelibrary.com). DOI: 10.1002/cnm.2522

Reproduction of pressure field in ultrasonic-measurement-integrated simulation of blood flow

Kenichi Funamoto*,† and Toshiyuki Hayase

Institute of Fluid Science, Tohoku University, 2-1-1 Katahira, Aoba-ku, Sendai 980-8577, Japan

SUMMARY

Ultrasonic-measurement-integrated (UMI) simulation of blood flow is used to analyze the velocity and pressure fields by applying feedback signals of artificial body forces based on differences of Doppler velocities between ultrasonic measurement and numerical simulation. Previous studies have revealed that UMI simulation accurately reproduces the velocity field of a target blood flow, but that the reproducibility of the pressure field is not necessarily satisfactory. In the present study, the reproduction of the pressure field by UMI simulation was investigated. The effect of feedback on the pressure field was first examined by theoretical analysis, and a pressure compensation method was devised. When the divergence of the feedback force vector was not zero, it influenced the pressure field in the UMI simulation while improving the computational accuracy of the velocity field. Hence, the correct pressure was estimated by adding pressure compensation to remove the deteriorating effect of the feedback. A numerical experiment was conducted dealing with the reproduction of a synthetic three-dimensional steady flow in a thoracic aneurysm to validate results of the theoretical analysis and the proposed pressure compensation method. The ability of the UMI simulation to reproduce the pressure field deteriorated with a large feedback gain. However, by properly compensating the effects of the feedback signals on the pressure, the error in the pressure field was reduced, exhibiting improvement of the computational accuracy. It is thus concluded that the UMI simulation with pressure compensation allows for the reproduction of both velocity and pressure fields of blood flow.

Received 10 April 2012; Revised 27 July 2012; Accepted 21 September 2012

KEY WORDS: bio-fluid mechanics; computational fluid dynamics; ultrasonic measurement; color Doppler imaging; measurement-integrated simulation

1. INTRODUCTION

Circulatory diseases such as heart disease and cerebrovascular disease are major causes of death. *In vivo* and *in vitro* experiments and numerical simulations of blood flow have been extensively carried out, indicating the relationships between diseases and hemodynamics [1, 2]. Blood flow information acquired by medical imaging techniques, such as ultrasonic measurement, magnetic resonance imaging (MRI) and computed tomography (CT), or directly measured by a catheter, sphygmomanometer or electrocardiogram is limited. On the other hand, blood flow simulation provides detailed information on three-dimensional unsteady hemodynamics including wall shear stress and pressure distributions. However, as it is inherently difficult to correctly specify the boundary and initial conditions, the computational results may differ from the real blood flow field data [3, 4]. Several methods have been proposed for flow simulation using defective boundary conditions, in which only flow rates are known [5, 6]. However, their efficiency for blood flow in a complicated

*Correspondence to: Kenichi Funamoto, Institute of Fluid Science, Tohoku University, 2-1-1 Katahira, Aoba-ku, Sendai 980-8577, Japan.

†E-mail: funamoto@reynolds.ifs.tohoku.ac.jp

vessel configuration remains to be investigated. Other factors, such as assumption of a rigid vessel wall, and uncertainties in vessel geometry, physical properties, and the model of the blood rheology, can also introduce errors into the computation. Consequently, at present, the diagnosis of circulatory diseases depends on empirical knowledge with limited measurement data. An innovative technique for accurate and detailed reproduction of blood flow field in a blood vessel is needed to realize more accurate and reliable diagnoses.

Various methodologies have been developed to computationally reproduce a flow field by integrating measurement and computation to overcome individual disadvantages. These methods include a method using proper orthogonal decomposition [7,8], data assimilation based on Tichonov regularization [9], least-squares finite element methods [10, 11], the Kalman filter [12], variational methods [13, 14], and measurement-integrated (MI) simulation [15–18]. Data assimilation based on four-dimensional variation is widely used, especially in numerical weather forecasting [14]. However, it requires huge computational resources to repeatedly solve flow dynamics and its adjoint, and therefore, is not suitable for application to problems of real-time flow reproduction. In contrast, the Kalman filter and MI simulation are rather simple methods sequentially comparing the computational result with the corresponding measurement data and directly feeding back the differences to the numerical simulation. Compared with the Kalman filter, which usually employs a low-dimensional linear model, the MI simulation, which uses computational fluid dynamics as a mathematical model, can provide a solution with high accuracy once a convergent result is obtained although there is no systematic design method of the feedback signal. The authors have applied MI simulation to blood flow analysis by integrating medical measurement (ultrasonic measurement or phase-contrast MRI) and numerical simulation [19,20]. With ultrasonic-measurement-integrated (UMI) simulation, the blood flow field is analyzed by applying artificial body forces proportional to the differences between the measured and computed Doppler velocities of the blood flow. Figure 1 shows a block diagram of the UMI simulation. Note that a 'Pressure compensation' block is newly added in this paper as explained in the following section. In our previous studies, a two-dimensional UMI simulation using real ultrasound color Doppler images was conducted [19]. The transient and steady characteristics of UMI simulation and the efficiency of feedback to reproduce unsteady three-dimensional hemodynamics were investigated by numerical experiments [21–23]. Those studies revealed that the UMI simulation improved computational accuracy in comparison with the ordinary simulation, making the computational velocity vector field approach that of a model solution of real blood flow. However, the reproducibility of the pressure field was not necessarily satisfactory [21,24].

In this study, reproduction of the pressure field by UMI simulation was investigated. In the second section of this paper, the effect of feedback based on Doppler velocity on the pressure field is first examined by theoretical analysis, and a pressure compensation method is derived. In the third section, results of the theoretical analysis and the proposed pressure compensation method are validated by a numerical experiment dealing with a synthetic three-dimensional steady flow in a thoracic aneurysm.

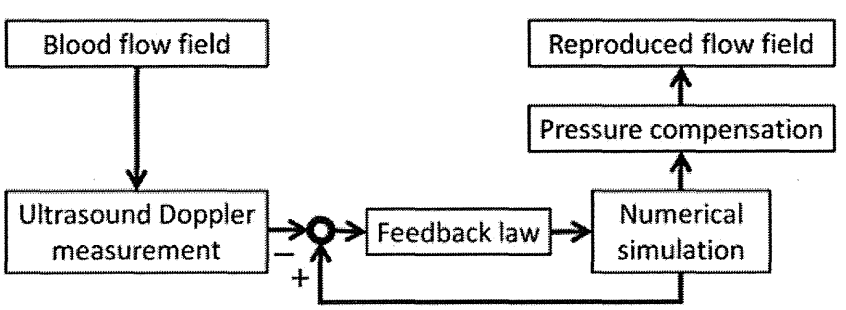

Figure 1. Block diagram of the UMI simulation.

DOI: 10.1002/cnm

2. THEORETICAL ANALYSIS

The effect of the feedback signal on the pressure field in the UMI simulation is clarified by theoretical analysis, and a pressure compensation method is developed.

2.1. Effect of feedback signals on the pressure field

The governing equations of the UMI simulation of blood flow in a blood vessel are the Navier–Stokes equations and the equation of continuity.

$$\rho\left(\frac{\partial \mathbf{u}}{\partial t}+(\mathbf{u}\cdot\nabla)\,\mathbf{u}\right)=\mu\Delta\mathbf{u}-\nabla p+\mathbf{f}, \tag{1}$$

$$\nabla\cdot\mathbf{u}=0, \tag{2}$$

where $\mathbf{u}=(u,\ v,\ w)$ is the velocity vector, p is the pressure, ρ is the density, μ is the viscosity, t is the time, and $\mathbf{f}=(f_x,\ f_y,\ f_z)$ is the external force term corresponding to the feedback signal. By substituting Equation (2) into the divergence of Equation (1), the pressure equation is derived as follows:

$$\Delta p=-\nabla\cdot\rho(\mathbf{u}\cdot\nabla)\,\mathbf{u}+\nabla\cdot\mathbf{f}. \tag{3}$$

Equations (1) and (3) are employed as the governing equations in the following analysis.

Regarding the boundary conditions, correct velocity profiles are assumed to be unknown, and a uniform or parabolic parallel profile with a known flow volume and free flow condition are specified at the upstream and downstream boundaries, respectively. The initial flow condition is an arbitrary flow field.

The feedback signal, $\mathbf{f}$, in Equation (1) is an artificial body force, which is proportional to the difference between the computed and measured Doppler velocities in the feedback domain defined in the computational domain:

$$\mathbf{f}=-K_{\mathrm{v}}^{*}\frac{\mathbf{\Phi}_d(\mathbf{u}-\mathbf{u}_{\mathrm{s}})}{U}\left(\frac{\rho U^2}{L}\right), \tag{4}$$

where K_{v}^{*} is the feedback gain (nondimensional), U is the characteristic velocity, L is the characteristic length, and $\mathbf{u}_{\mathrm{s}}$ is the velocity vector of the real blood flow. $\mathbf{\Phi}_d$ $(d=1,\ 2,\ 3)$ is a projection function of a three-dimensional vector to the d-dimensional subspace [21]. The projection of the three-dimensional velocity vector in the direction of the ultrasonic beam in the UMI simulation corresponds to the case of $d=1$, and $\mathbf{\Phi}_1(\mathbf{u})$ and $\mathbf{\Phi}_1(\mathbf{u}_{\mathrm{s}})$ correspond to computed and measured Doppler velocities, respectively. Here, measurement errors, such as noise, contained in ultrasonic Doppler measurement are ignored for simplicity. Note that, in our previous study [23], the effects of major measurement errors on the computational accuracy of the UMI simulation were investigated, and methods to compensate those effects were proposed. The special case with $K_{\mathrm{v}}^{*}=0$ corresponds to the ordinary numerical simulation without feedback.

Previous studies [21–23] have revealed that with a proper application of feedback, the computational velocity field approaches the real velocity field of the blood flow. Generally, because a velocity field has a unique pressure field, it was expected that the computational pressure field would concurrently approach the real pressure field. However, the reproducibility of pressure field was not necessarily satisfactory.

The pressure field by the UMI simulation is discussed in the following. The velocity field, $\mathbf{u}_{\mathrm{s}}$, and the pressure field, p_{s}, of a real blood flow satisfy governing Equations (1) and (3) without the external force term, $\mathbf{f}$, with the upstream and downstream boundary conditions of the correct velocity profiles and with the initial condition of the correct velocity vector field at the first time step:

$$\rho\left(\frac{\partial \mathbf{u}_{\mathrm{s}}}{\partial t}+(\mathbf{u}_{\mathrm{s}}\cdot\nabla)\,\mathbf{u}_{\mathrm{s}}\right)=\mu\Delta\mathbf{u}_{\mathrm{s}}-\nabla p_{\mathrm{s}}, \tag{5}$$

$$\Delta p_{\mathrm{s}}=-\nabla\cdot\rho(\mathbf{u}_{\mathrm{s}}\cdot\nabla)\,\mathbf{u}_{\mathrm{s}}. \tag{6}$$

DOI: 10.1002/cnm

In the UMI simulation, incorrect specification of boundary conditions introduces error to the computational result as compared with the real blood flow, but the feedback based on Doppler velocity works to reduce the error in the velocity vector field in the feedback domain. Therefore, in the equation derived from the subtraction of Equation (6) from Equation (3), the velocity vector, $\mathbf{u}$, is approximately equal to the real velocity vector, $\mathbf{u}_s$, and the following equation is approximately satisfied in the feedback domain:

$$\Delta p = \Delta p_s + \nabla \cdot \mathbf{f}. \tag{7}$$

This equation implies that the pressure field, p, of the UMI simulation becomes different from the real pressure field, p_s, because of the effect of feedback in the case that the divergence of the feedback force vector is not zero.

2.2. *Pressure compensation method*

A pressure compensation method for the UMI simulation is introduced. The pressure compensation is applied after the convergent results of velocity and pressure are obtained (see Figure 1). The correct pressure field, p_s, is expressed as the summation of the computational result, p, and the compensation term, p_f.

$$p_s = p + p_f. \tag{8}$$

With Equation (7) and Equation (8) operated by Laplacian operator, the following equation is obtained.

$$\Delta p_f = -\nabla \cdot \mathbf{f}. \tag{9}$$

The pressure compensation, p_f, is calculated from Equation (9) by setting zero value at the boundaries of the computation domain. In the case that the blood flow is considered to be parallel flow such as the one in a straight blood vessel, pressure is constant over the cross-section perpendicular to the flow. In addition, if the flow rate in the UMI simulation is identical to that of the real flow, the pressure differences between upstream and downstream boundaries are the same between the cases. Consequently, the boundary conditions of the pressure equations for p and p_s can be considered to be the same. Because $p_f = p_s - p$ from Equation (8), the value of p_f should be zero at the upstream and downstream boundaries. By substituting the pressure compensation, p_f, into Equation (8), an estimated value, p'_s, of the correct pressure is obtained.

The proposed pressure compensation method is equivalent to a modification of the UMI simulation retaining only the divergence-free part of the feedback signal, $\mathbf{f}_{div}$. The feedback signal, $\mathbf{f}$, can be decomposed to an irrotational part, $\mathbf{f}_{irr}$, and a divergence-free part, based on Helmholtz decomposition [25]. Pressure compensation, p_f, obtained from Equation (9) determines the irrotational part of the feedback signal as $\mathbf{f}_{irr} = -\nabla p_f$, which does not contribute to improvement of the computational accuracy of the velocity field, but deteriorates that of the pressure field.

2.3. *Discretization*

Outlines of discretization of the governing equations of the UMI simulation, including the pressure compensation equation, are described in this section. The above-mentioned governing equations are discretized by means of the finite volume method and are solved with the SIMPLER method [26]. The concrete notations of the parameters in the following equations, and supplementary pressure correction equations and velocity correction procedure in the SIMPLER method, are explained in [26].

The x-directional momentum equation in Navier–Stokes equations of Equation (1):

$$B_p u_{i,j,k} = \sum B_{nb} u_{nb} + S_{i,j,k} + A_i (p_{i-1,j,k} - p_{i,j,k}) + \Delta V_{i,j,k} f_{x_{i,j,k}}, \tag{10}$$

where Bs are the elements of the matrix consisting of all of the diffusive terms and a part of the convective terms in the discretized Navier–Stokes equation, and $(\sum B_{nb} u_{nb})$ is the summation of

DOI: 10.1002/cnm

the values at six adjacent nodes in the three-dimensional computation. The second term, $S_{i,j,k}$, on the right side is the source term, which consists of a part of the convective terms and a part of the time-derivative term. The third term is the pressure gradient term in which A_i is the cross-sectional area of the control volume, and the last term is the feedback term in which $\Delta V_{i,j,k}$ is the volume of the cell. Subscript p denotes the position where $u(i,\ j,\ k)$ is defined, and nb means adjacent nodes. Equations for y-directional and z-directional momentums are analogous to that in Equation (10).

The pressure equation of Equation (3):

$$C_P p_{i,j,k} = \sum C_{nb} p_{nb} + S_{p_{i,j,k}} + S_{f_{i,j,k}}, \tag{11}$$

where Cs are the elements of the matrix derived from discretization of the pressure equation, $S_{pi,j,k}$ is the source term derived from discretization of the first term on the right side of Equation (3), and $S_{fi,j,k}$ is the source term because of the feedback. Subscript P denotes the position where $p(i,\ j,\ k)$ is defined. The source term because of the feedback, $S_{fi,j,k}$, is denoted in the following equation:

$$S_{f_{i,j,k}} = \frac{\rho}{B_p}[(f_{x\,i,j,k} - f_{x\,i+1,j,k})A_i + (f_{y\,i,j,k} - f_{y\,i,j+1,k})\,A_j + (f_{z\,i,j,k} - f_{z\,i,j,k+1})A_k], \tag{12}$$

where A_i, A_j, and A_k are the cross-sectional areas of the control volume facing each direction.

Pressure compensation for feedback of Equation (9):

Equation (9) is also expressed in a way similar to the pressure equation

$$C_p p_{f_{i,j,k}} = \sum C_{nb} p_{f_{nb}} - S_{f_{i,j,k}}, \tag{13}$$

where coefficients C_p and C_{nb}, and the source term $S_{fi,j,k}$ are identical with those in Equations (11) and (12).

3. VALIDATION WITH NUMERICAL EXPERIMENT

Results of the theoretical analysis and the proposed pressure compensation method are validated by a numerical experiment dealing with a synthetic three-dimensional steady flow in a thoracic aneurysm. Ultrasonic measurement provides the Doppler velocity necessary for the feedback in UMI simulation, but it does not provide other information necessary for evaluating the UMI simulation such as three-dimensional velocity vectors or pressure field. Hence, we do not use real measurement data for the reference data. Instead, we use a numerical solution for a synthetic steady flow with realistic upstream and downstream velocity boundary conditions called 'standard solution' as a model of real blood flow to perform the numerical experiment. The boundary conditions of the standard solution are determined from a preliminary simulation of blood flow in a whole aorta including an aneurysm. Reproduction of the standard solution by the UMI simulations with/without the pressure compensation and the ordinary numerical simulation without feedback are investigated. The numerical simulations conducted in this section are summarized in Table I.

Table I. Classification of preliminary simulation (PS), standard solution (SS), UMI simulation (UMIS), and ordinary simulation (OS).

Name	Solver	Domain	Grid	Boundary velocity	Feedback	Note
PS	FLUENT	Whole aorta Figure 2(a)	Hexahedral 142,417	Uniform inlet Free stream outlet	N/A	Boundary velocity for SS was obtained.
SS	Original (SIMPLER)	Aneurysm Figure 2(b)	Orthogonal $40 \times 34 \times 49$	Specified velocity inlet & outlet	N/A	Model of real flow
UMIS	Original (SIMPLER)	Aneurysm Figure 2(b)	Orthogonal $40 \times 34 \times 49$	Uniform inlet Free stream outlet	Applied	Measurement data was was generated by SS.
OS	Original (SIMPLER)	Aneurysm Figure 2(b)	Orthogonal $40 \times 34 \times 49$	Uniform inlet Free stream outlet	N/A	

DOI: 10.1002/cnm

3.1. Methods

A numerical experiment was conducted to investigate the computational accuracy of the pressure field by the UMI simulation and to examine the efficiency of the proposed pressure compensation method. The objective was a steady flow in a thoracic aneurysm, which was the same as in a previous study [22]. A steady numerical solution with realistic boundary conditions was first defined as the standard solution. The boundary conditions of the standard solution were determined from a preliminary simulation of blood flow in a whole aorta including the aneurysm. Although generation of synthetic measurement data for validation of new algorithms has been investigated [27, 28], the computational three-dimensional velocity vectors were simply projected in the direction of the ultrasonic beam without consideration of measurement errors to obtain the Doppler velocity of the standard solution. Then, with inaccurate boundary conditions but with the correct flow volume, UMI simulation and an ordinary simulation without feedback were performed. In the UMI simulation, Doppler velocities of the standard solution were used for feedback. After the convergent results of velocity and pressure were obtained, the pressure compensation was applied to the pressure field (see Figure 1).

A preliminary simulation for a whole aorta was first performed. The configuration of the whole aorta from the ascending aorta to the abdominal aorta, including an aneurysm in the descending aorta, was reconstructed, as shown in Figure 2(a), by accumulating X-ray CT images (Aquilion 16, Toshiba, Tokyo, Japan) of a 76-year-old female patient with commercial three-dimensional reconstruction software (Mimics 7.3, Materialise, Leuven, Belgium) [22]. A preliminary simulation of a steady blood flow in the whole aorta (Figure 2(a)) was carried out by using commercial computational fluid dynamics software (FLUENT 6.1.22, Fluent, Inc., Lebanon, NH). The computational grid used in the preliminary FLUENT simulation consisted of 142,417 hexahedral elements. Pressure–velocity coupling was accomplished by the SIMPLE method, and spatial discretization schemes were employed as follows: a Green-Gauss cell-based scheme for gradient; a standard scheme for pressure; and a first-order upwind for momentum. Uniform velocity was applied at the inlet boundary so that the average flow rate became 8.65×10^{-5} m^3/s, and a

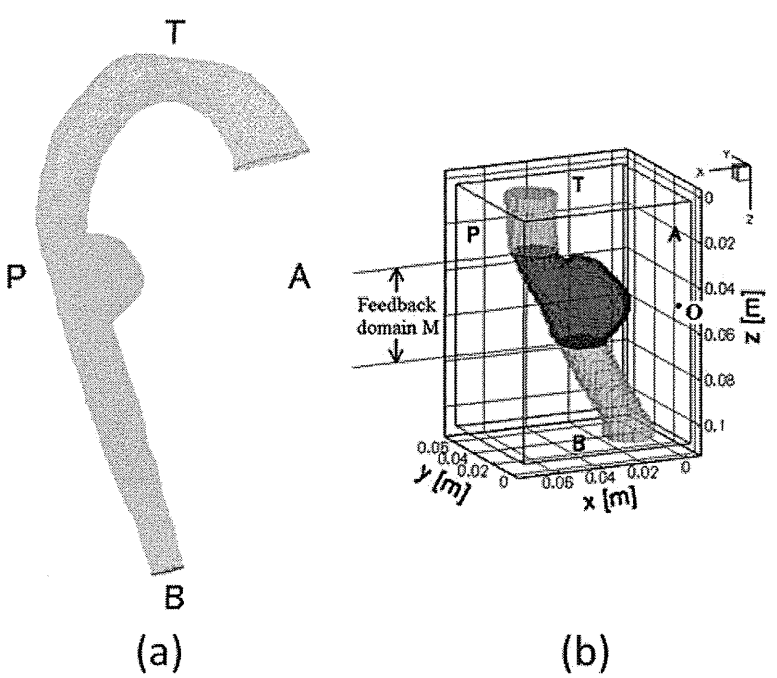

Figure 2. Computational grids for (a) a preliminary simulation of a steady flow in the whole aorta with an aneurysm in the descending aorta by using FLUENT, and for (b) the other simulations of the flow in the partial domain including the aneurysm with a feedback domain (dark gray zone) and a probe position at O.

DOI: 10.1002/cnm

free-flow condition was applied at the downstream boundary. A no-slip condition was set on the wall. The convergence criterion in the numerical simulation was set at 1×10^{-4} for momentum and continuity equations.

In the following computations for the standard solution, the UMI simulation, and the ordinary simulation, the computational domain was limited to the vicinity of the thoracic aneurysm, as shown in Figure 2(b). A computational grid system was generated by introducing a staggered grid system of $40 \times 34 \times 49$ grid points in x, y, and z directions, compromising reproducibility of vessel configuration and computational load. The grid interval dz in the z direction was set at 2.00×10^{-3} m, which was the same as the slice interval of the X-ray CT, and those in the other directions were determined to be $dx = dy = 1.78 \times 10^{-3}$ m. The equivalent diameter of the blood vessel, D, at the upstream boundary calculated by averaging x-directional and y-directional maximum lengths of the cross-section of the blood vessel at the upstream boundary was 23.47×10^{-3} m. Flow rate was set at 8.65×10^{-5} m^3/s (same as the preliminary simulation), and the average flow velocity at the upstream boundary, U, was 2.00×10^{-1} m/s. The density, ρ, and viscosity, μ, of the blood were assumed to be 1.00×10^3 kg/m^{3}and 4.00×10^{-3} Pa $\cdot$ s, respectively. All the variables were nondimensionalized with the equivalent diameter of the blood vessel, D, as the characteristic length, L, the average flow velocity as the characteristic velocity, U, and the density of blood, ρ, as the characteristic density. The Reynolds number of the steady flow was 1174. From here on, the same symbols are used for both dimensional and nondimensional values because it does not cause any confusion.

In the computation of the standard solution, velocity profiles at the upstream and downstream boundaries were determined as those on the corresponding cross-sections of the preliminary simulation. In the UMI simulation and the ordinary simulation, a uniform parallel flow was applied at the upstream boundary, and the free flow condition was set at the downstream boundary.

Because the computational result converges to the target flow with the aid of the feedback process, unsteady flow computation is required for the UMI simulation even for the present steady target flow. Time-dependent computation was performed for all cases. The computational time increment was set as $\Delta t = 0.01(1.17 \times 10^{-3}$ s) [22].

In UMI simulation, considering the acquisition of Doppler velocities in the three-dimensional domain by transesophageal ultrasonography, the ultrasound probe or the origin of ultrasonic beam was set at O[$(x, y, z) = (0.008, 0.023, 2.045)$((0.000 m, 0.001 m, 0.048 m))], which was located at the same height as the aneurysm, as shown in Figure 2(b). The Doppler beam direction was along a line from the origin of ultrasonic beam to each computational gird point. Blood flow in the whole aneurysmal domain M[$1.193 \leqslant z \leqslant 2.897$(0.028 m $\leqslant z \leqslant$ 0.068 m), shown by a dark gray zone in Figure 2(b)], including the parent blood vessel, was assumed to be measured. Domain M was defined as the feedback domain, and at all the grid points in the fluid region of domain M, feedback signals were added to the UMI simulation based on the differences of Doppler velocities between the simulation and the standard solution.

In the computation of the standard solution, the UMI simulation and the ordinary simulation, the governing equations were discretized by the finite volume method and were solved with an original program based on the SIMPLER method [26, 29] as described in the previous section. The convective terms were discretized with the reformulated QUICK scheme [30], and the time derivative terms were discretized with the first Euler implicit scheme. Linear algebraic equations were solved using the modified strongly implicit (MSI) scheme [31]. The convergence criterion in the numerical simulation was set at 1×10^{-4} for momentum and continuity equations.

To evaluate the computational accuracy of the UMI simulation and the ordinary simulation, a space-averaged error norm of a variable, a (velocity vector, $\mathbf{u}$, or pressure, p), in a monitoring domain Ω was defined by the following equation:

$$\bar{e}_\Omega(a,t) = \frac{1}{N} \sum_{X_n \in \Omega} \left| \frac{a_{cn}(t) - a_{sn}(t)}{a_{\mathrm{ref}}} \right|, \tag{14}$$

where n and N are the identification number and the total number of the monitoring points, respectively, $|\cdot|$ is the absolute value for scalar variables or the l_1 norm, $|u| + |v| + |w|$, for velocity vector $\mathbf{u}$, and a_{ref} is the characteristic value for normalization: $a_{\mathrm{ref}} = U$ for velocity or $a_{\mathrm{ref}} = \rho U^2$

DOI: 10.1002/cnm